Original article

A Cost-Effective IMU-Based Wave Buoy: Customizable Design, Performance Variability, and Field Trial

Yu. Yu. Yurovsky ✉, **O. B. Kudinov**

Marine Hydrophysical Institute of RAS, Sevastopol, Russian Federation
✉ *y.yurovsky@mhi-ras.ru*

Abstract

Purpose. The objective of the study is to present a small batch of wave-measuring buoys developed at Marine Hydrophysical Institute (MHI) using affordable inertial sensors and to evaluate potential errors in wave height measurements associated with random variations in sensor parameters.

Methods and Results. Based on one of the most common sensors, the MPU9250, several identical wave buoys were constructed: 10 in a small housing with a 300 mAh battery for short-term (up to 24 hours) manual measurements and 3 in a larger housing with a 12000 mAh battery for longer deployments (up to a month). Laboratory tests provided upper estimates of linear distortions and measurement biases for the accelerometer, gyroscope, and magnetometer. A field experiment was conducted at the MHI's Black Sea Hydrophysical Subsatellite Polygon, where three prototype buoys were used to take measurements at two locations: near the shore (30 m from shore, 4 m depth) using both small and large buoys, and near the Stationary Oceanographic Platform (500 m from shore, 30 m depth) using a large buoy, alongside a reference resistive wave gauge. Measurements were taken over two days during easterly winds, with peak speeds reaching 16 m/s. The maximum recorded significant wave height was 1.2 m. Laboratory error estimates for the constructed sensors fall within the ranges specified by the manufacturer. The most critical error for wave height measurements – accelerometer calibration – was no more than 2% for the component normal to the sensor housing and no more than 0.5% for orthogonal components (one of which was used as the vertical axis in the buoys). Field measurements near the platform showed agreement with reference wave gauge data for significant wave heights with a root-mean-square error of 2.4 cm. Wave elevation spectra obtained near the shore by two buoys matched within 95% confidence intervals (a similar agreement was observed between the buoy and wave gauge measurements near the platform). However, wave heights near the shore and near the platform differed by a factor of 2–3 during the experiment, which cannot be attributed to sensor parameter variations and instead reflects the inhomogeneity of the surface wave field.

Conclusions. The developed wave buoys, based on low-cost inertial motion units, can be effectively used in swarm deployments, and factory variations in their internal parameters do not hinder the reliable measurement of typical wind waves. Thus, the proposed approach is useful for studying wave transformation mechanisms at coastal boundaries and for adapting wave models to specific water areas.

Keywords: wave buoy, inertial motion unit, significant wave height, wind waves, measurement errors, field validation, coastal Black Sea

Acknowledgments: Buoy prototyping and calibration were sponsored by the Russian Scientific Foundation grant 24-27-00153 "Measuring waves with small buoys: methods, validation, prospects of miniaturization". Wind wave field analysis was sponsored by the MHI State Order FNNN2024-0001.

For citation: Yurovsky, Yu.Yu. and Kudinov, O.B., 2026. A Cost-Effective IMU-Based Wave Buoy: Customizable Design, Performance Variability, and Field Trial. *Physical Oceanography*, 33(1), pp. 201-214.

Introduction

Amid the continuous widening of technical means for sea surface wave observations [1–3], measuring surface wave parameters by analyzing buoy motion has been a standard oceanographic task for decades [4–6]. A well-established global industry produces specialized wave-measuring buoys for routine ocean wave monitoring (https://datawell.nl/categories/buoys/, https://www.sofarocean.com/products/spotter) [7–9]. Nevertheless, in recent years, there has been a growing trend toward buoys developed by small research teams [10–15]. This approach allows for custom instrument design tailored to specific research objectives, such as studying wave-current interactions [11], wave-ice dynamics [12, 16], short wave research [10, 17], air-sea interactions [14], or satellite calibration [13]. These developments have been made possible by rapid advancements in microelectronics, particularly the widespread adoption of microelectromechanical (MEMS) inertial sensors, which are now used across various scientific and engineering fields.

In this study, we share our experience in developing wave-measuring buoys based on such sensors. Today, manufacturers, including Russian ones, offer a wide range of inertial sensors, with prices varying by orders of magnitude depending on measurement accuracy. Factory calibration errors in accelerometer channels typically do not exceed 2–3% for the simplest models, making them suitable for wave height measurements (e.g., https://invensense.tdk.com/products/motion-tracking/9-axis/mpu-9250). This is because the statistical error in significant wave height estimates is usually higher (around 5–6% for 30-minute averaging [18]), and, these errors can be further reduced through additional calibration if necessary.

While the noise level of inertial sensors largely dictates their cost, it has been shown [19] that the primary source of errors lies in the nonlinearity of the coordinate transformation between moving and stationary reference frames, whereas the sensor intrinsic noise plays a minor role.

Given these considerations, modern out-off-the-shelf inertial motion units appear to be a viable option for deploying fleets (or swarms) of simple, uniform measuring devices designed for research tasks requiring distributed measurements. Examples include studying wave field inhomogeneities in currents [20], shallow-water effects [21], or nonlinear processes in coastal [22] and [23] shelf zones.

The purpose of this paper is to present a prototype wave buoy based on the MPU9250, one of the simplest and most affordable inertial motion units. A small test batch of these buoys was produced to assess potential parameter variations. A field experiment demonstrated one possible application scenario involving simultaneous wave measurements taken in the coastal zone and approximately 500 m offshore.

Buoy design and measurement method

The buoy operates on the principle of a data logger, collecting measurements from an inertial sensor and saving them to a memory card with timestamps from its built-in real-time clock. A deliberate rejection of full autonomy allowed us to design the electronic components in an extremely simple configuration (Fig. 1). All parts except the power source are mounted on a custom-designed printed circuit board (PCB). The key component is the MPU9250 inertial sensor (a combined accelerometer, gyroscope, and magnetometer) positioned along the PCB axis of

symmetry at the point where resonant pitch/roll motions are minimized. The sensor is controlled by an ATMega328P microcontroller, which initializes the MPU9250 upon startup, polls it at 100 Hz, and records raw measurements to a microSD card inserted into the onboard slot. To prevent aliasing effects, the sampling rate is set to 100 Hz, more than twice the selected bandwidth of 41 Hz.

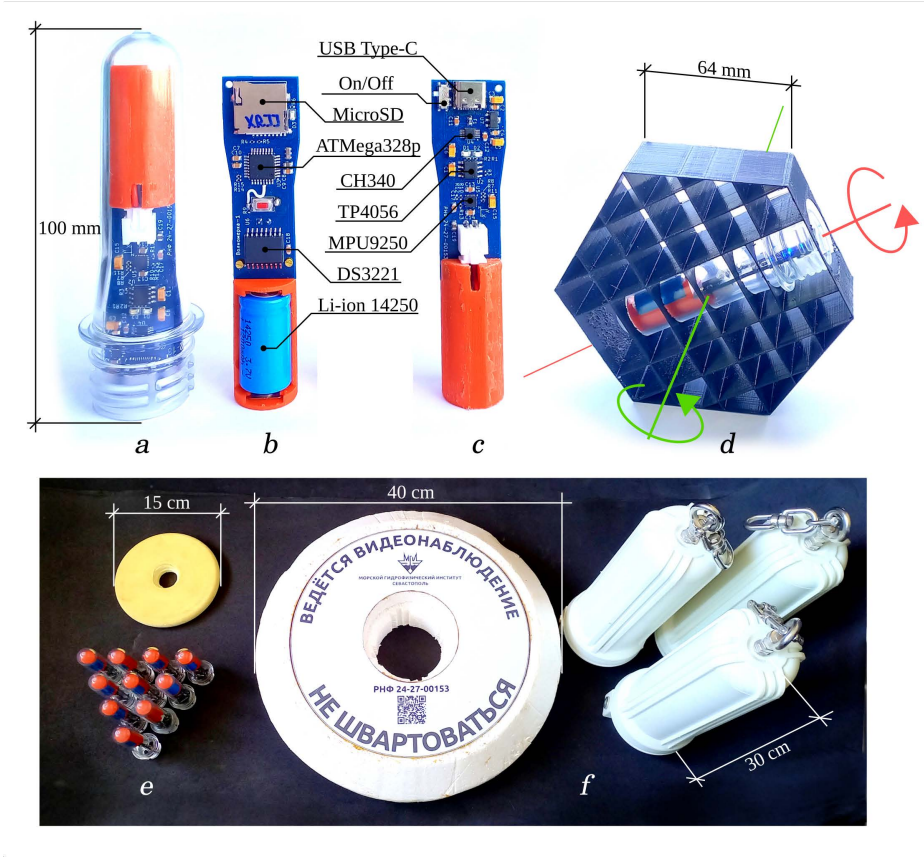

F i g. 1. Buoy design: printed circuit board (PCB) inside a small hull (*a*); front (*b*) and rear (*c*) views of the standalone buoy PCB; 3D-printed prism for IMU calibration (*d*); ten small-hull buoys with 15-cm floats (*e*); three large-hull buoys with 40-cm floats (*f*)

The board also includes a DS3231 real-time clock for synchronizing recordings with the World time. The start time of each measurement session is embedded in the filename of the corresponding data file. A USB Type-C port is provided for battery charging (via a TP4056 charge controller) and, when needed, firmware updates and microcontroller debugging (using a CH340 interface). A microswitch, placed in an easily accessible location, allows the user to power the device on and off. Each buoy is assigned a unique four-character identifier, derived from the hash sum of the microcontroller factory serial number.

The main PCB is 70 mm long with a variable width (17.5 mm at its narrowest and 21.5 mm at its widest), ensuring a secure fit inside a hermetically sealed capsule made from a standard PET preform (PC12245), commonly used in food packaging.

The remaining space inside the capsule is occupied by a 14250 lithium-ion battery housed in a 3D-printed plastic holder. With a nominal capacity of 300 mAh and an average current consumption of 18 mA, the battery provides at least 16 hours of continuous operation.

The sealed capsule weighs 50 g when fully assembled, giving it slight positive buoyancy but also resulting in low natural oscillation frequencies (fractions of 1 Hz), which fall within the range of typical wave energy. To improve buoyancy and stability on water, foam floats (15 mm thick and 15 cm in diameter, with adjustable dimensions depending on requirements) are attached. The bottom of the capsule features a sealed stainless-steel eyelet for securing a holding line.

In this configuration, the buoy is particularly well-suited for manual deployments, such as ship-based wave measurements. For longer-term observations, the housing can be easily enlarged to accommodate a higher-capacity battery without modifying the electronics. As an example of an alternative design, this study also tested a standard 10SL polypropylene casing (commonly used in water treatment systems) paired with 40-cm-diameter foam floats (10 cm thick). This version holds six 18650 lithium-ion batteries connected in parallel, providing a total capacity of approximately 12000 mAh. Combined with the more robust housing, this setup allows for moored deployments lasting about one month.

The buoy records raw measurements from the inertial sensor onto the memory card, specifically the three components of the acceleration vector (in the range of ±2g, with a resolution of 2^{16}), rotation rate (±500 deg/s, 2^{16}), and magnetic field (±4800 uT, 2^{10}). During the post-processing, this data is used to calculate wave parameters.

It should be noted that by preserving the raw, unprocessed data, a researcher gains the ability to perform highly flexible and transparent processing. As an example, this study employs one of the most popular methods for estimating hull orientation, the Kalman filter (an open-source implementation [24] was used, https://ahrs.readthedocs.io/en/latest/filters/ekf.html), which takes acceleration, rotation rate, and magnetic field recordings as input. The processing output consists of hull rotation matrices tied to world coordinates for each timestamp. These matrices are used to compute vertical acceleration which, in turn, are applied to estimate frequency of sea surface elevations, following the standard techniques [4, 18].

Results and discussion

Laboratory tests. The availability of multiple identical sensors allows for estimating (essentially comparing with specifications) potential variations in characteristics that affect surface wave measurements. The noise properties of the sensors used were analyzed in detail in [19]. Therefore, this study focuses primarily on the accuracy of scale (calibration) factors and zero offsets. To assess these parameters, it is sufficient to apply a known input signal to the sensor and analyze the output measurements.

The principles of such calibration are well-established. For instance, the Earth's magnetic field serves as a reference signal for the magnetometer, as it remains nearly constant during measurements. The sensor is randomly oriented so that, in its reference frame, the magnetic field vector covers the widest possible solid angle

(ideally 4π). In an ideal scenario, the endpoints of the measured magnetic field vectors should form a sphere with a radius equal to the field strength. In reality, this shape deviates from a sphere and is better approximated by an ellipsoid, assuming linear distortions

$$\begin{bmatrix} q_x \\ q_y \\ q_z \end{bmatrix} = \begin{bmatrix} A_{xx} & A_{xy} & A_{xz} \\ A_{xy} & A_{yy} & A_{yz} \\ A_{xz} & A_{yz} & A_{zz} \end{bmatrix} \cdot \left(\begin{bmatrix} p_x \\ p_y \\ p_z \end{bmatrix} - \begin{bmatrix} B_x \\ B_y \\ B_z \end{bmatrix} \right),$$

where **p** is the measured data vector, **B** is the offset vector, A is the linear distortion matrix, and **q** is the true data vector.

The accelerometer, magnetometer and gyroscope calibration examples are shown in Fig. 2. The ellipsoid coefficients can be easily determined by solving an overdetermined system of equations using the least squares method (Fig. 2, *b*), see the numerical implementation of this procedure [1] (https://www.mathworks.com/help/nav/ref/magcal.html) used in this study. In wave measurements, the magnetic field is only used to estimate the buoy orientation. Thus, the absolute value of the measured field is irrelevant.

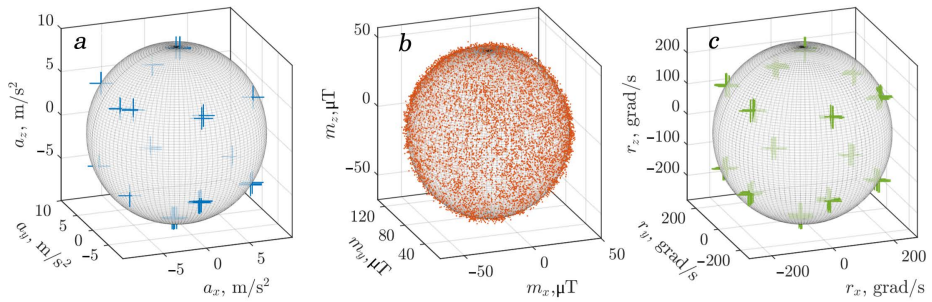

F i g. 2. Calibration example for the accelerometer (*a*), the magnetometer (*b*), and the gyroscope (*c*) using the THRJ buoy sample. The measured data points (dots and crosses) and the fitted ellipsoids are shown

A similar calibration can be performed for the accelerometer, using the precisely known acceleration due to gravity as the reference signal. Unlike the magnetic field, it is crucial to avoid additional accelerations, so the sensor must remain stationary during each measurement. The procedure was as follows. Each sample (a PCB with a battery in a capsule) was mounted inside a 3D-printed hexagonal prism (Fig. 1, *d*), which was sequentially placed on a stationary table on each of its faces for 30 seconds. After a full rotation, the capsule was rotated inside the prism by 60 degrees around its axis, and the measurements were repeated. This process accumulated 36 measurements with the gravity vector applied to the sensor's proof masses from different directions. Only 14 of them are virtually independent, but this is quite enough to estimate the distortion coefficients and

[1] Ozyagcilar, T., 2012. *Calibrating an eCompass in the Presence of Hard and Soft-Iron Interference*. Freescale Semiconductor, pp. 1-17.

offsets similarly to magnetometer calibration (Fig. 2, *a*). Note that the exact angular positioning was not critical for determining the desired parameters; the key factor was ensuring the widest possible coverage of all orientations.

Gyroscopic distortion (Fig. 1, *c*) was assessed in a similar manner, using a fixed frame but on a turntable. The applied rotation rate was determined by the periodicity of changes in the magnetic field. The gyroscope offsets were estimated from more precise static sensor measurements.

The calibration results for all sensors are summarized in Table, which shows the elements of linear distortion matrix A and offsets **B**. Note that the deviation of the diagonal matrix elements from unity is typically less than 1% for the accelerometer, around 1% for the gyroscope, and approximately 2–3% for the magnetometer. The cross-axis distortion coefficients, A_{xy}, A_{xz}, A_{yz}, for all three types of sensors are generally below 1%.

Laboratory test results

Sensor ID	$(A_{xx}-1)\cdot100$	$(A_{yy}-1)\cdot100$	$(A_{zz}-1)\cdot100$	$A_{xy}\cdot100$	$A_{xz}\cdot100$	$A_{yz}\cdot100$	B_x	B_y	B_z	V
Accelerometer, m/s²										
XDJJ	−0.738	0.306	0.437	−0.284	0.068	0.012	0.240	0.057	−0.049	9.867
XWDJ	−0.659	0.377	0.286	−0.213	−0.094	−0.013	0.303	0.132	−0.070	9.863
XVZJ	−0.659	0.377	0.286	−0.213	−0.094	−0.013	0.303	0.132	−0.070	9.863
V5Z2	−0.696	0.296	0.404	−0.028	−0.051	−0.018	−1.294	0.371	0.144	9.869
THRJ	−0.706	0.367	0.344	−0.235	−0.259	0.024	0.127	0.075	0.026	9.866
XRJJ	−0.591	0.400	0.194	0.302	−0.146	0.026	0.226	0.222	−0.113	9.852
SDTJ	−0.664	0.258	0.410	−0.044	−0.134	−0.074	0.505	0.147	−0.174	9.866
T9U2	−0.712	0.335	0.380	−0.098	0.095	−0.003	0.234	0.073	−0.011	9.855
XDV2	−1.115	0.560	0.565	−0.063	−0.042	0.007	−0.395	0.118	−0.193	9.890
UZK2	−0.673	0.247	0.430	−0.096	0.187	0.077	−0.111	0.116	−0.009	9.862
TDK3	−0.505	0.345	0.163	0.048	−0.258	0.004	−1.076	0.303	0.030	9.852
XZ4W	−0.041	−0.255	0.297	0.207	−0.066	0.005	0.049	0.074	−0.161	9.848
ZZR5	0.219	−0.338	0.119	−0.079	0.003	−0.006	0.230	−0.345	−0.334	9.850
Magnetometer, uT										
XDJJ	−2.442	3.742	−1.167	0.887	−0.621	−1.252	13.5	99.7	−33.8	55.6
XWDJ	0.462	3.064	−3.418	0.047	0.391	0.212	72.8	−9.0	5.1	57.1
XVZJ	−5.827	2.449	3.690	0.488	−0.895	1.742	48.4	70.0	−16.7	54.1
V5Z2	−2.054	3.901	−1.712	1.338	−0.795	−0.234	54.1	77.9	−45.4	54.6
THRJ	−1.774	3.788	−1.908	0.400	0.115	−0.089	68.1	80.0	−4.2	54.7
XRJJ	−1.797	3.257	−1.370	0.469	−0.501	0.897	118.8	−5.9	−32.1	55.0
SDTJ	−2.231	4.319	−1.942	0.464	−0.016	−0.935	−28.5	80.7	−40.0	56.4
T9U2	−3.148	3.901	−0.593	0.388	0.049	−1.827	13.1	57.5	−52.0	56.1
XDV2	−1.059	3.048	−1.912	−0.495	0.644	0.319	63.2	−30.4	38.5	55.5
UZK2	−2.622	2.808	−0.107	0.435	0.406	−0.342	−8.4	−43.7	−99.7	55.4
TDK3	2.360	−2.093	−0.210	−0.595	−0.594	−0.131	53.1	−37.0	−7.1	54.2
XZ4W	8.152	−6.457	−1.118	0.583	−1.769	−0.647	27.0	10.0	14.6	55.4
ZZR5	2.912	−3.436	0.636	−0.861	−0.022	−0.298	69.9	−35.8	31.6	54.8
Gyroscope, grad/s										
XDJJ	−0.125	−0.409	0.539	−0.218	0.427	−0.057	0.355	0.464	−1.152	279.235
XWDJ	−0.177	−0.659	0.843	−0.185	−0.188	0.049	0.076	2.072	−0.018	277.963
XVZJ	−0.335	−0.510	0.851	−0.010	0.082	0.006	0.135	0.265	1.904	279.040
V5Z2	−0.273	0.010	0.268	−0.155	−0.676	0.080	−0.042	0.475	−1.815	278.299
THRJ	−1.606	0.207	1.426	−0.550	−0.106	0.124	0.381	0.735	0.968	277.055
XRJJ	1.499	−2.616	1.171	0.201	0.255	−0.107	−0.272	2.373	−0.009	275.973
SDTJ	0.013	−0.428	0.417	−0.062	0.227	−0.043	−0.373	1.190	−1.565	277.952
T9U2	0.057	−0.023	−0.033	−0.281	0.152	0.041	−0.299	0.931	−1.271	278.882
XDV2	−0.726	0.195	0.539	−0.237	0.539	0.071	−0.637	0.334	−0.454	280.026
UZK2	0.006	−0.585	0.583	0.086	−0.231	−0.020	−0.390	−0.264	0.913	279.148
TDK3	0.090	−0.456	0.439	0.420	−0.264	2.616	−4.128	−1.345	−2.309	337.545
XZ4W	0.382	−0.310	0.063	0.181	−0.216	−3.646	1.505	−0.400	0.961	340.983
ZZR5	0.210	−1.584	1.399	−0.146	−0.367	0.222	−5.232	−0.317	−0.921	334.538

It is worth noting that for wave measurements, linear distortions in acceleration along one of the axes, which becomes vertical in the final product (in our case, the *y*-axis), may be particularly significant. Offsets are less critical in terms of their impact on wave estimates, as they are subtracted from the signals during the processing, similar to the standard calibration procedure for magnetometric data. The most critical factor may be the gyroscope offset, as such distortions could be falsely interpreted by the processing algorithm as a rotation of the body around a particular sensor axis. In all our cases, the gyroscope offsets were below 2.5 grad/s, while the maximum value specified in the sensor datasheet is 5 grad/s.

Fig. 3 shows the test results for the magnetometer, accelerometer, and gyroscope channels in separate scatter plots, with distortion coefficients, $\left[A_{ii} \cdot q_i^{est}/q_i^{true}\right]^{-1}$, and offsets B_i plotted on the axes (where i denotes the x, y, or z axis). The parameters here q_i^{est} and q_i^{true} represent the calibrated vector length and its reference value respectively: for the accelerometer, it is the known free-fall acceleration (9.81 m/s²); for the gyroscope – the rotation rate determined from the number of sensor revolutions per time unit; for the magnetometer, where the true field is unknown, q_i^{true} is taken as the mean measured value across all samples.

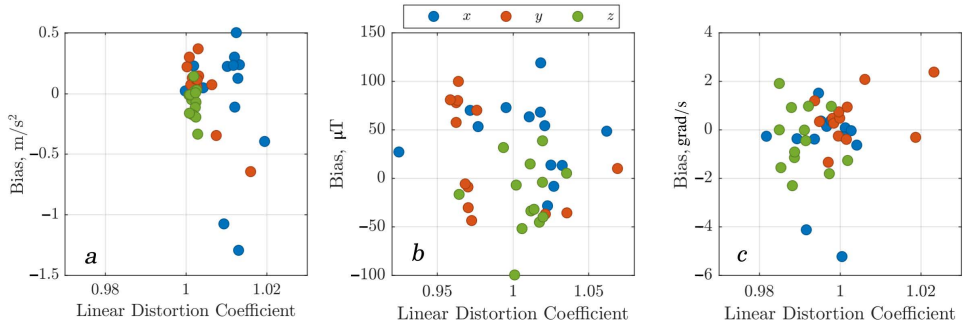

F i g. 3. Scatter plots of linear distortion coefficients along the selected color-coded axis and offsets for accelerometer (*a*), magnetometer (*b*), gyroscope (*c*)

As can be seen, all values are distributed more or less randomly, except for the accelerometer, where measurements along the *x*-axis (the axis normal to the sensor and the board) exhibit noticeably higher distortions. Though there is weak systematic bias towards acceleration overestimation, the maximum distortions never exceed 2% in terms of relative acceleration errors. The core of *z*-axis acceleration distortions, the most important for wave height estimation, is concentrated within the 0–0.5% interval (0.2% on average). For two sensors, the accelerometer offset magnitude exceeds the permissible limits (more than 1 m/s², compared to the datasheet specification of 0.784 m/s²), but their linear distortions remain within acceptable bounds.

The error statistics obtained from a small batch of 13 sensors fall within the manufacturer's specified limits. It should be emphasized that such measurements (conducted without specialized precision equipment or test benches) are only

approximate. However, the results can thus be interpreted as the upper bound of the confidence interval within which the true distortion coefficients and offsets fall.

Field Experiment. Three units of the aforementioned sensors were deployed in a field experiment aimed at demonstrating their practical application. The measurements were conducted in September 2024 at the Black Sea Hydrophysical Subsatellite Polygon of Marine Hydrophysical Institute during a persistent easterly wind event lasting several days. Data was collected at two locations (Fig. 4).

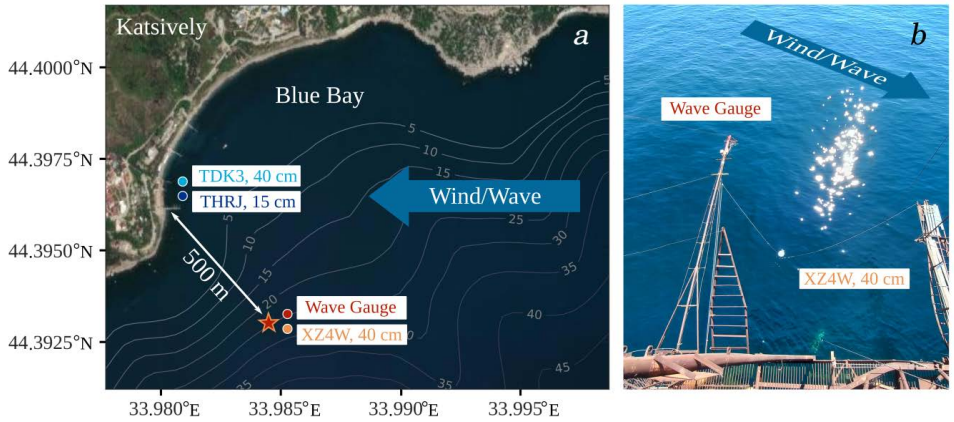

F i g. 4. Experimental setup overview: *a* – satellite image of the Black Sea Hydrophysical Subsatellite Polygon of MHI with overlaid ETOPO1 bathymetry, showing schematic positions of the TDK3, THRJ, and XZ4W buoys, and wave gauge installation points (indicated by color-coded symbols); *b* – the XZ4W buoy deployed from the platform using a double-line attachment, alongside a wave gauge. The arrow indicates the prevailing easterly wind and wave direction

In the coastal zone, approximately 30 meters from the shoreline, the TDK3 buoy (40 cm diameter) was anchored for 48 hours at ~ 4 m water depth. Nearby, the THRJ buoy (15 cm diameter) was manually deployed for short measurement sessions (several hours), remaining within 10 m of TDK3. Approximately 500 m offshore, measurements were taken using the XZ4W buoy (identical in design to TDK3) deployed from the Stationary Oceanographic Platform at ~ 30 m water depth. The platform was equipped with a six-channel resistive wave gauge [25, 26], whose measurements served as reference data.

Since the buoy deployment was conducted under unfavorable weather conditions (making it impossible to use a boat for anchored setups), the buoy near the platform was deployed from an 11-meter boom on a bifilar suspension to prevent the mooring line from twisting around the platform structures and surrounding instruments. A similar deployment method was used in the coastal zone: the buoy was stretched between the end of a pier and a concrete block on the shore, ensuring it remained approximately at the same place during measurements.

This deployment approach is advantageous as it eliminates the need for a boat entirely. However, it introduces anisotropy in the buoy horizontal motions (movement along the line connecting the suspension points is constrained),

complicating wave direction estimation. For this reason, only wave energy characteristics are analyzed in this study.

Throughout the experiment, a consistent easterly wind was observed, almost uniform in direction but variable in speed (Fig. 5). Wind speeds reached 8 m/s on the first day (September 14) and 16 m/s on the following day (September 15), gradually subsiding by the morning of September 16 with a particular 180º turnaround event just after midnight. The significant wave height measured by the reference wave gauge at the platform followed wind patterns accordingly, peaking at 0.8 m on the first day and 1.2 m on the second.

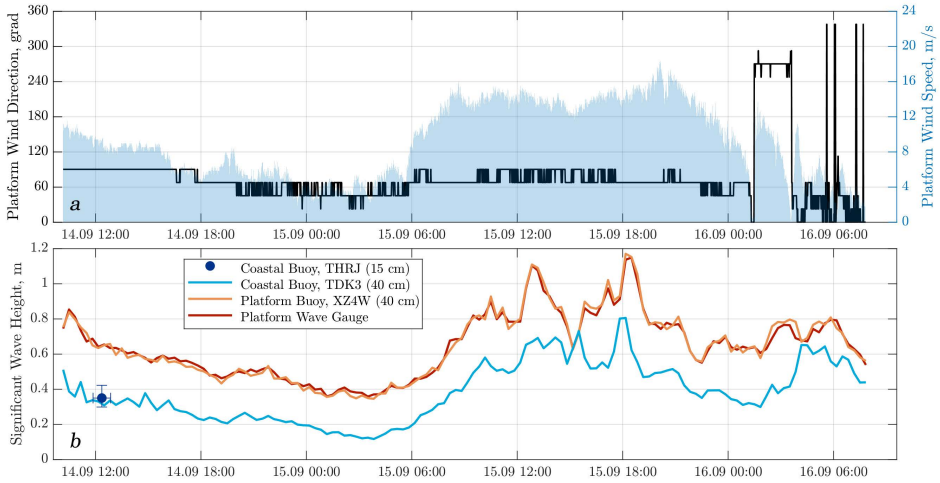

F i g. 5. Wind speed and direction (*a*) and significant wave height (*b*) during the experiment: measurements from the platform (reddish) and coastal (blue) stations by buoys and wave gauges. Gray shading and black line indicate wind speed and direction measured at the platform

Despite the unconventional deployment setup, wave height measurements showed excellent agreement with the reference wave gauge data (Fig. 5, reddish lines) throughout the experiment. The buoy XZW4 exhibited a root-mean-square deviation of just ~ 2.4 cm relative to the wave gauge, with a bias of ~ 0.1 cm and a correlation coefficient of 0.992.

Wave heights measured by the nearshore buoy TDK3 (Fig. 5, blue line) followed a similar trend. However, a notable reduction in wave heights was observed near the shore, averaging approximately 1.5–3 times lower than the deeper-water measurements near the platform. An exception occurred around 15:00 on September 15, when wave heights near the platform were temporarily lower, briefly equalizing the measurements. Toward the end of the wind event on September 16, wave heights became more comparable between the two locations: 0.6 m nearshore and 0.8 m near the platform, clearly indicating the dominant swell contribution (the unstable wind direction also supports the general fading of the wave event).

The observed differences clearly cannot be attributed to sensor parameter variations, which in our case amount to fractions of a percent. This conclusion is further supported by parallel measurements taken manually from shore using

the 15-cm buoy THRJ in the coastal zone near the TDK3 buoy. Despite differences in hull dimensions, mass, and buoyancy characteristics, the wave height measurements taken around noon on September 14 fall within the statistical variation range of measurements made by buoy TDK3 (Fig. 5, blue symbol).

A more detailed comparison of measurements from all three buoys and the wave gauge is presented in Fig. 6, which shows frequency spectra of wave elevations. The spectra are displayed in both linear and logarithmic scales to better visualize the energy-carrying and short-wave components. The spectra recorded by different buoys at coastal station showed close agreement, consistent with the parameter variability observed in laboratory tests (blueish lines). Specifically, the spectra fell within mutual confidence intervals. Discrepancies between TDK3 and THRJ were confined to the high-frequency range, attributable to differences in hull geometry (different hull sizes exhibit distinct amplitude-frequency responses). As evident from Fig. 6, *a*, these variations had negligible impact on the energy-carrying portion of wave spectrum. Similarly, spectra from the 40-cm XZ4W buoy and the wave gauge at the platform location also agreed within confidence intervals.

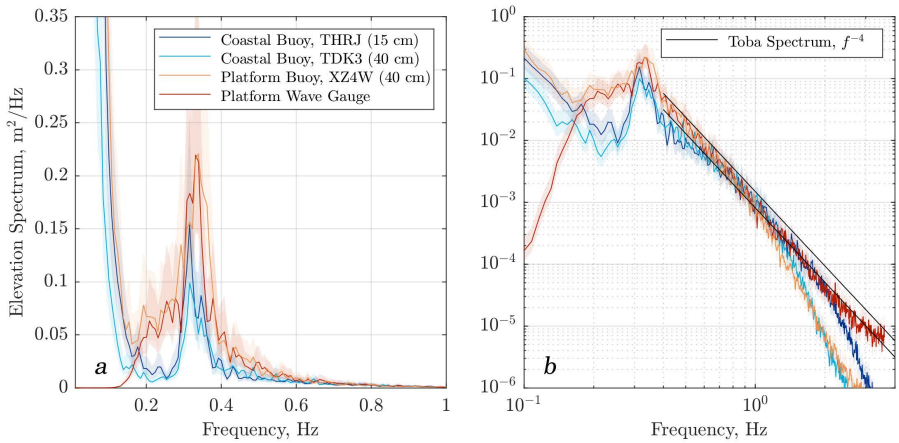

F i g. 6. Elevation spectra recorded by buoys and a wave gauge on the first day (midday, September 14, 2024) in linear (*a*) and logarithmic (*b*) scales. Color shading indicates 95% confidence interval for the spectra. The Toba spectrum parameterization [27] is shown for reference

In contrast, pronounced differences emerged between the coastal and platform location measurements. The ratio of spectral energy densities at the 0.30–0.35 Hz peak reached ~ 2 (wave amplitude ratio ~ 1.4). This peak is not attenuated uniformly: its high-frequency component (~ 0.325–0.35 Hz) decays more rapidly than the low-frequency one (~ 0.30–0.325 Hz). This selective attenuation causes an unexpected downshift in the peak frequency as waves propagate shoreward. While simple statistical scattering may be a prosaic cause, an alternative speculative explanation is that the sub-peaks correspond to waves from different directions, which consequently experience differing degrees of shadowing at the coastal site.

Within the 0.2–0.25 Hz band, the wave gauge spectra at the platform clearly exhibited swell. Comparable spectral levels in this range were observed in the XZ4W

buoy data. The energy ratio between nearshore and platform measurements was approximately one order of magnitude (wave amplitudes ratio ~ 3). This represents a lower-bound estimate of the ratio, as the swell-associated spectral peak was obscured by low-frequency noise in buoy records. As noted earlier [19, 28], this artifact stems from methodological constraints in deriving elevation from acceleration data (double integration, or the ω^{-4} multiplier in frequency domain), not sensor quality. The absence of artificial low-frequency suppression resulted in prominent spectral distortions below ~ 0.12 Hz.

Another observed distinction was the spectral slope. Despite similar peak characteristics, typical of young wave regimes (e.g., the well-known JONSWAP parameterization [29]), the slope at the coastal location (−3.5) was markedly gentler than the platform location's "standard" slope (−4). Empirical and theoretical explanations for this trace back to classical works in the field (e.g., [30, 31]), with ongoing experimental investigations. Particularly relevant is [32], where buoy-based analyses of wind-wave spectra under short-fetch conditions were conducted farther offshore.

The systematic differences in both wave spectra and significant wave heights are evidently related to the physics of wave transformation in shallow water (wave reflection and dissipation) and may also be associated with other local effects, such as diffraction near coastal structures, seafloor features, distortion of the wind field near the shore, and similar factors. A detailed discussion of these issues falls well beyond the scope of this work. Nevertheless, the presented pilot study demonstrates that the proposed equipment and methodology can be effectively used to study wave field inhomogeneities both in the open sea and in the coastal zone, while the Black Sea Hydrophysical Subsatellite Polygon can serve as a convenient location for such studies, since even over short distances one can observe rather strong contrasts in wave parameters.

Conclusion

The paper presents the experience of batch developing a wave buoy based on simple and readily available components. The main element is an inertial motion unit (MPU9250, a combined accelerometer/gyroscope/magnetometer), which signals are recorded onto a memory card without any preprocessing, with synchronization to a built-in real-time clock. All components, except the power source, are assembled on a specially designed printed circuit board, allowing for easy production of small batches of identical measuring devices if necessary.

For the tests presented in this work, 10 small buoys were manufactured with a 300 mAh battery (15-cm float, for manual measurements up to 1 day), as well as 3 larger buoys with a 12000 mAh battery capacity (40-cm float, for deployments of up to 1 month). Using simple mechanical rigs, an upper error estimate and the spread of linear distortion coefficients were obtained for a sample of 13 sensors used. These parameters were found to be within the limits specified in the manufacturer documentation. For example, the most important parameter for measuring wave heights – the accuracy of acceleration measurements – was no worse than 2%, compared to the declared maximum of 3% (on average, 1% for the component normal to the housing and 0.2% for orthogonal components). The reported method

for estimating the upper error limit can be used for express-testing of buoys, including in field conditions without expensive laboratory equipment.

A field experiment was conducted using several buoys from the presented set. One large buoy was deployed near the Stationary Oceanographic Platform, where a resistive string wave gauge was also installed. A second large buoy of the same type was placed near the shore, where intermittent measurements were taken with a third small buoy. Close agreement between wave parameters near the platform (40-cm buoy and wave gauge), as well as near the shore (40-cm buoy and 15-cm buoy), indicates the reliability of the data obtained from the developed buoys. At the same time, significant differences were observed in the spectra near the platform and near the shore. For example, the swell energy (at ~ 0.2 Hz) near the shore was 10 times lower than near the platform, while the energy of waves corresponding to the wind peak (~ 0.35 Hz) decreased only twofold when approaching the shore indicating the strong shallow-water effects in the wave field captured by the experimental setup.

Thus, this work demonstrates the feasibility of distributed wave measurements using buoys based on a very simple and affordable hardware platform.

REFERENCES

1. Ivonin, D.V., Myslenkov, S.A., Chernyshov, P.V., Arkhipkin, V.S., Telegin, V.A., Kuklev, S.B., Chernyshova, A.Y. and Ponomarev, A.I., 2013. Monitoring System of Wind Waves in Coastal Area of the Black Sea Using Coastal Radars, Direct Wave Measurements and Modeling: First Results. *Regional Environmental Issues*, (4), pp. 172-182 (in Russian).
2. Ermoshkin, A.V., Bogatov, N.A., Kapustin I.A. and Molkov, A.A., 2024. Determination of the Significant Wave Height from Doppler Radar Images of the Sea Surface. *Oceanology*, 64 (Suppl. 1), pp. S29-S37. https://doi.org/10.1134/S000143702470084X
3. Yurovsky, Yu.Yu., Malinovsky, V.V., Korinenko, A.E., Glukhov, L.A. and Dulov, V.A., 2023. Prospects for Radar Monitoring of Wind Speed, Wind Wave Spectra and Velocity of Currents from an Oceanographic Platform. *Ecological Safety of Coastal and Shelf Zones of Sea*, (3), pp. 40-54.
4. Longuet-Higgins, M.S., Cartwright, D.E. and Smith, N.D., 1961. Observations of the Directional Spectrum of Sea Waves Using the Motions of a Floating Buoy. In: NAS, 1961. *Ocean Wave Spectra: Proceedings of a Conference, Easton, Maryland, May 1–4, 1961*. Englewood Cliffs: Prentice-Hall, pp. 111-132.
5. Gryazin, D.G., 2000. [*Calculation and Design of Buoys for Sea Wave Measuring*]. Saint Petersburg: SPbGITMO(TU), 134 p. (in Russian).
6. Cavaleri, L., Alari, V., Benetazzo, A., Björkqvist, J.-V., Breivik, Ø., Davis, J., Hope, G., Kleven, A., Leirvik, F. [et al.], 2025. More Room at the Top: How Small Buoys Help Reveal the Detailed Dynamics of the Air-Sea Interface. *Bulletin of the American Meteorological Society*, 106(6), pp. E1063-E1076. https://doi.org/10.1175/BAMS-D-24-0120.1
7. Steele, K., Lau, J. and Hsu, Y.-H., 1985. Theory and Application of Calibration Techniques for an NDBC Directional Wave Measurements Buoy. *IEEE Journal of Oceanic Engineering*, 10(4), pp. 382-396. https://doi.org/10.1109/JOE.1985.1145116
8. Herbers, T.H.C., Jessen, P.F., Janssen, T.T., Colbert, D.B. and MacMahan, J.H., 2012. Observing Ocean Surface Waves with GPS-Tracked Buoys. *Journal of Atmospheric and Oceanic Technology*, 29(7), pp. 944-959. https://doi.org/10.1175/JTECH-D-11-00128.1
9. Raghukumar, K., Chang, G., Spada, F., Jones, C., Janssen, T. and Gans, A., 2019. Performance Characteristics of "Spotter," a Newly Developed Real-Time Wave Measurement Buoy. *Journal of Atmospheric and Oceanic Technology*, 36(6), pp. 1127-1141. https://doi.org/10.1175/JTECH-D-18-0151.1

10. Yurovsky, Yu.Yu. and Dulov, V.A., 2017. Compact Low-Cost Arduino-Based Buoy for Sea Surface Wave Measurements. In: IEEE, 2017. *Progress in Electromagnetics Research Symposium.* Singapore: PIERS, pp. 2315-2322. https://doi.org/10.1109/PIERS-FALL.2017.8293523

11. Veras Guimarães, P., Ardhuin, F., Sutherland, P., Accensi, M., Hamon, M., Pérignon, Y., Thomson, J., Benetazzo, A. and Ferrant, P., 2018. A Surface Kinematics Buoy (SKIB) for Wave–Current Interaction Studies. *Ocean Science*, 14(6), pp. 1449-1460. https://doi.org/10.5194/os-14-1449-2018

12. Rabault, J., Nose, T., Hope, G., Muller, M., Oyvind, B., Voermans, J., Hole, L.R., Bohlinger, P., Waseda, T., 2022. OpenMetBuoy-v2021: An Easy-to-Build, Affordable, Customizable, Open-Source Instrument for Oceanographic Measurements of Drift and Waves in Sea Ice and the Open Ocean. *Geosciences*, 12(3), 110. https://doi.org/10.13140/RG.2.2.15826.07368

13. Mironov, A.S. and Charron, L., 2023. Miniaturized Drifting Buoy Platform for the Creation of Undersatellite Calibration and Validation Network. In: IEEE, 2023. *OCEANS 2023 – Limerick.* Limerick, Ireland: IEEE, pp. 1-10.

14. Thomson, J., Bush, P., Castillo Contreras, V., Clemett, N., Davis, J., De Klerk, A., Iseley, E., Rainville, E.J., Salmi, B. [et al.], 2024. Development and Testing of MicroSWIFT Expendable Wave Buoys. *Coastal Engineering Journal*, 66(1), pp. 168–180. https://doi.org/10.1080/21664250.2023.2283325

15. Hope, G., Seldal, T.I., Rabault, J., Bryhni, H.T., Bohlinger, P., Björkqvist, J.-V., Nordam, T., Kleven, A., Mostaani, A., 2025. SFY – A Lightweight, High-Frequency, and Phase-Resolving Wave Buoy for Coastal Waters. *Journal of Atmospheric and Oceanic Technology*, 42(2), pp. 133-154. https://doi.org/10.1175/JTECH-D-23-0170.1

16. Kodaira, T., Katsuno, T., Nose, T., Itoh, M., Rabault, J., Hoppmann, M., Kimizuka, M. and Waseda, T., 2023. An Affordable and Customizable Wave Buoy for the Study of Wave-Ice Interactions: Design Concept and Results from Field Deployments. *Coastal Engineering Journal*, 66(1), pp. 74–88. https://doi.org/10.1080/21664250.2023.2249243

17. Yurovsky, Yu.Yu. and Dulov, V.A., 2020. MEMS-Based Wave Buoy: Towards Short Wind-Wave Sensing. *Ocean Engineering*, 217, 108043. https://doi.org/10.1016/j.oceaneng.2020.108043

18. Earle, M.D., 1996. *Nondirectional and Directional Wave Data Analysis Procedures*. NDBC Technical Document 96-01. Slidell, USA: Stennis Space Center, 43 p.

19. Yurovsky, Yu.Yu. and Kudinov, O.B., 2025. Methods and Errors of Wave Measurements Using Conventional Inertial Motion Units. *Physical Oceanography*, 32(1), pp. 63-83.

20. Sullivan, P.P. and McWilliams, J.C., 2010. Dynamics of Winds and Currents Coupled to Surface Waves. *Annual Review of Fluid Mechanics*, 42(1), pp. 19-42. https://doi.org/10.1146/annurev-fluid-121108-145541

21. Kuznetsov, S. and Saprykina, Y., 2021. Nonlinear Wave Transformation in Coastal Zone: Free and Bound Waves. *Fluids*, 6(10), 347. https://doi.org/10.3390/fluids6100347

22. Saprykina, Y., 2020. The Influence of Wave Nonlinearity on Cross-Shore Sediment Transport in Coastal Zone: Experimental Investigations. *Applied Sciences*, 10(12), 4087. https://doi.org/10.3390/app10124087

23. Divinsky, B.V. and Kuklev, S.B., 2022. Experiment of Wind Wave Parameter Research on the Black Sea Shelf. *Oceanology*, 62(1), pp. 8-12. https://doi.org/10.1134/S0001437022010040

24. Hartikainen, J., Solin, A. and Särkkä, S., 2008. Optimal Filtering with Kalman Filters and Smoothers – A Manual for Matlab Toolbox EKF/UKF. *Biomedical Engineering*, pp. 1-57.

25. Bondur, V.G., Dulov, V.A., Murynin, A.B. and Yurovsky, Yu.Yu., 2016. A Study of Sea-Wave Spectra in a Wide Wavelength Range from Satellite and In-Situ Data. *Izvestiya, Atmospheric and Oceanic Physics*, 52(9), pp. 888-903. https://doi.org/10.1134/S0001433816090097

26. Smolov, V.E. and Rozvadovskiy, A.F., 2020. Application of the Arduino Platform for Recording Wind Waves. *Physical Oceanography*, 27(4), pp. 430-441. https://doi.org/10.22449/1573-160X-2020-4-430-441

27. Toba, Y., 1972. Local Balance in the Air-Sea Boundary Processes. *Journal of the Oceanographical Society of Japan*, 28(3), pp. 109-120. https://doi.org/10.1007/BF02109772

28. Ashton, I.G.C. and Johanning, L., 2015. On Errors in Low Frequency Wave Measurements from Wave Buoys. *Ocean Engineering*, 95, pp. 11-22. https://doi.org/10.1016/j.oceaneng.2014.11.033

29. Hasselmann, K., Barnett, T.P., Bouws, E., Carlson, H., Cartwright, D.E., Enke, K., Ewing, J.A., Gienapp, H., Hasselmann, D.E. [et al.], 1973. *Measurements of Wind-Wave Growth and Swell Decay during the Joint North Sea Wave Project (JONSWAP)*. Hamburg: Deutches Hydrographisches Institut. Reiche A (8), Nr. 12, 95 p.

30. Phillips, O.M., 1958. The Equilibrium Range in the Spectrum of Wind-Generated Waves. *Journal of Fluid Mechanics*, 4(4), pp. 426-434. https://doi.org/10.1017/S0022112058000550

31. Zakharov, V.E., 2010. Energy Balance in a Wind-Driven Sea. *Physica Scripta*, T142, 014052. https://doi.org/10.1088/0031-8949/2010/T142/014052

32. Rybalko, A., Myslenkov, S. and Badulin, S., 2023. Wave Buoy Measurements at Short Fetches in the Black Sea Nearshore: Mixed Sea and Energy Fluxes. *Water*, 15(10), 1834. https://doi.org/10.3390/w15101834

Submitted 08.07.2025; approved after review 13.08.2025;
accepted for publication 10.11.2025.

About the authors:

Yury Yu. Yurovsky, Leading Researcher, Head of the Applied Sea Physics Laboratory, Marine Hydrophysical Institute of RAS (2 Kapitanskaya Str., Sevastopol, 299011, Russian Federation), CSc. (Phys.-Math), **Scopus Author ID: 24377122700**, **ORCID ID: 0000-0002-9995-3965**, **ResearcherID: F-8907-2014**, **SPIN-code: 8482-5777**, y.yurovsky@mhi-ras.ru

Oleg B. Kudinov, Researcher, Marine Hydrophysical Institute of RAS (2 Kapitanskaya Str., Sevastopol, 299011, Russian Federation), CSc. (Tech.), **SPIN-code: 2248-7034**, obk91@mail.ru

Contribution of the co-authors:

Yury Yu. Yurovsky – development of methodology and conducting experimental research, data processing, analysis, description of research results, writing original draft

Oleg B. Kudinov – development and manufacturing of measuring devices, conducting experimental research, reviewing and editing the text

The authors have read and approved the final manuscript.
The authors declare that they have no conflict of interest.